Simulation-based evaluation of single pass continuous diafiltration with alternating permeate flow direction

Ruijie Tan[1], Matthias Franzreb[1*]

[1]Institute of Functional Interfaces (IFG), Karlsruhe Institute of Technology (KIT), Eggenstein-Leopoldshafen, Karlsruhe, 76344

Correspondence concerning this article should be addressed to Matthias Franzreb at matthias.franzreb@kit.edu

Abstract

In the framework of modern bioprocessing continuous ultrafiltration/diafiltration (UF/DF) is getting increasingly popular. However, while continuous UF can be easily implemented using a so-called single pass tangential flow filtration (SPTFF) module, continuous DF requires a more complicated setup including several SPTFF modules and intermittent dilution steps. Recently, we introduced a novel module design for continuous DF allowing simultaneous delivery of fresh buffer while withdrawing the permeate, thus achieving high degrees of buffer exchange within a single unit. In addition, the system allows to cyclically switch the flow direction of DF buffer through the membranes. Those uncommon features, however, also make it more difficult to determine an operation optimum experimentally by means of trial and error. Therefore, here a detailed finite element model of the physical processes within the module is presented, predicting key figures such as the obtained diafiltration efficiency and the resulting pressures. Because within the module all flow channels are filled by a 3D-printed porous grid supporting the membranes from both sides, the modified Brinkman equation was used to simulate the hydrodynamics, while common mass balance differential equations including accumulation, convection, and an anisotropic dispersion term were used for the simulation of concentration profiles of dissolved species. The predicted key figures are in good agreement with experimental results, obtained for feed solutions including up to 50 g/L of protein and being operated with and without switching the flow direction of the diafiltration buffer. A thorough parameter study reveals that the module shows the best performance for unidirectional flow of the diafiltration buffer, reaching diafiltration efficiencies independence to the applied diavolumes which are comparable to the ones of a conventional multi-stage setup using three SPTFF modules. Therefore, the simulation-based evaluation of optimum operation conditions reveals that the new module design has the potential to realize truly continuous diafiltration setups with high efficiency, requiring only one unit and no extra external piping for returning diafiltration in counterflow. Such simplified setups should be especially useful in small, flexible processing plants as they are increasingly demanded in the biopharmaceutical industry.

Key Words: Diafiltration, Continuous processing, SPTFF, Modelling, Concentration profiles.

1 Introduction

Membrane-based separation processes, including microfiltration (MF), ultrafiltration (UF), diafiltration (DF), and reverse-/forward osmosis (RO/FO), are indispensable separation technologies in diverse fields such as biopharmacy, biotechnology, dairy industry or water treatment [1–4]. For the formulation of high value bioproducts, UF is usually used for concentrating the protein, while DF is used for exchanging the buffer in which the protein is dissolved. One limiting factor for the productivity of these processes is the fact that the retained molecules accumulate on the membrane surface [5] (Fig. 1A). During ultrafiltration, the accumulating process is undergoing two periods: concentration polarization (CP) and membrane fouling [6–9]. Concentration polarization occurs immediately when the filtration process starts, however, the formed proteinaceous layer is reversible and releases back into the bulk when the applied flux through the membrane is diminished. The accumulated proteins may change the effective MWCO of membrane, hence deteriorating the membranes hydraulic permeability and selectivity [10]. When the protein concentration at the membrane surface exceeds the solubility limit, irreversible fouling phenomena can be observed. Various types of membrane fouling have been reported, such as adsorption, pore-blocking, and deposition of solidified solute [8,11–13].
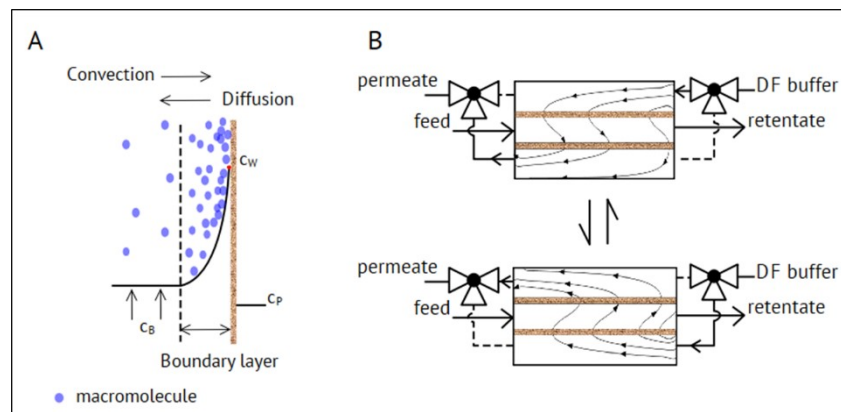

Fig. 1. Microscopic accumulation phenomena and macroscopic flow patterns in the newly developed single pass tangential flow filtration module. A. Concentration polarization of macromolecules at the surface of an ultrafiltration membrane. c_B: concentration of the macromolecules in the bulk; c_W: concentration at the membrane surface; c_P: concentration in the permeate stream. B. Diafiltration operation modes of a single pass tangential flow filtration module containing two membranes. The module can apply an alternating direction of the perfusion of diafiltration buffer as inherent backflush to reduce the concentration polarization effects.

The usual way to limit CP is the application of so-called tangential flow filtration. In this operation mode the feed solution is pumped in parallel to the membrane surface at high velocities, in order to reduce the thickness of the CP layer. The high velocities result in short residence times and only small diafiltration effects during this duration. Therefore, the retentate has to be recycled in a loop and pumped through the

module several times. In contrast, so-called single pass tangential flow filtration (SPTFF) uses only one pass of the feed solution. However, in this case the flow velocity has to be reduced strongly in order to achieve long enough residence times for efficient ultrafiltration [14–16]. If the systems are used for diafiltration, several of the modules are used with intermittent dilution steps with diafiltration (DF) buffer. The application of a single pass simplifies the setup and enables truly continuous operation. However, the low tangential flow velocities amplify the problem of concentration polarization. In order to reduce the accumulation phenomena, we recently developed a novel continuous single pass diafiltration system [17] (Fig. 1B). Within this system, the middle channel guiding the retentate flow is bounded by two membranes. By this, it is possible to supply fresh DF buffer and discharge the permeate at the same time and along the complete flow path of the retentate. This allows to reach high diafiltration efficiencies within a single module, while commercial SPTFF modules need a series of two, or in many cases three, modules and intermittent mixing steps in order to reach high diafiltration efficiency. In addition, the new system allows the optional operation mode of alternating direction of the perfusion of the membranes (see Fig. 1B). When the direction of perfusion is reversed during continuous operation, this acts as inherent backflush. Applying this operation mode and counter-current flow directions between the middle and the lateral flow channels a single module of this type is able to achieve a continuous diafiltration efficiency of more than 99% with a diavolume of 7.2.

Besides its effectiveness, the new SPTFF module containing two membranes offers a higher number of process parameters that can be controlled in order to optimize the performance for a specific diafiltration task. Next to the common parameters, such as feed flux and the applied diafiltration volumes, these include the choice between co-current or counter-current operation and the frequency of the optional switches of the perfusion direction through the membranes during continuous operation. Because of the additional complexity caused by the increased number of process parameters, the experiments also revealed that the duration until the quasi-stationary conditions of the process are fully developed may take a high number of switching intervals and therefore long times. In consequence, the experimental optimization of the process conditions of the new SPTFF module is a time consuming and laborious undertaking, which is why we decided to develop a simulation tool that predicts the performance of the system and allows a better understanding of its special properties.

Looking into literature, there is no model reported which would allow the simulation of a two-membrane system with simultaneous perfusion of fresh DF buffer and permeate discharge, as well as cyclic switches of the perfusion directions. Nevertheless, there exist several excellent publications about modelling approaches towards ultrafiltration, which represent the state-of-the-art and give helpful advice about modelling dynamic phenomena, such as concentration polarization. Those models have been used to predict

fluxes, pressure profiles, concentration distributions, shear stresses, and mass transfer as well as accumulation phenomena. Respective models are available for different setups, such as dead-end modules [3,8,18,19], flat sheet cross-flow rigs [20,21], hollow fiber modules [7,22] and multistage SPTFF units [23,24]. In the last two decades, the description of the accumulation phenomena during UF developed from a static, mostly qualitative to a dynamic quantitative analysis in order to better understand the important process limitations resulting. The development was accompanied by improved experimental technologies to visualize the accumulation process near the membrane [3]. In 2002, Ghosh [19] developed a pulse injection technique applying BSA to study membrane fouling. Later, Fernández-Sempere et al. [8] utilized holographic interferometry to visualize the effects of concentration polarization *in-situ*. They also predicted concentration profiles and permeate fluxes by modeling using an empirical equation based on the global convection-diffusion mechanism.

In contrast to the above mentioned global correlations, models based on computational fluid dynamics (CFD) using e.g. finite volume (FVM) or finite element (FEM) techniques enable to consider complex system geometries and predict local concentration and flow patterns [25]. Marcos et al. [22] presented a 2D FEM model using the software COMSOL Multiphysics (COMSOL Inc, Burlington, USA) to simulate transient flow and concentration profiles based on the equations of momentum and mass conservation for a hollow fiber cross-flow UF. They applied a resistance-in-series model to consider reversible as well as irreversible CP and fouling effects at the membrane surface. They also introduced an empirical correlation predicting a linear increase of the fluid viscosity with the concentration of the accumulated proteins. In a separate study by Schausberger et al. [21], also a 2D CFD model was used to assess the total flux and fouling by surface adsorption under various feed volume flows, pH and protein concentrations for UF using a flat-sheet cross flow rig. The results show that CP phenomena have to be considered even at low transmembrane fluxes, because otherwise significant membrane-solute-solvent interactions would be ignored. They suggested replacing the individual convection-diffusion equations for proteins and ionic species with alternative multi-component transport equations. The same point was also stressed by Rajabzadeh et al. [7] in their study introducing a model for hollow fiber cross-flow UF of soy protein extracts. Recently, Aguirre-Montesdeoca et al. [20] introduced the local critical flux to demonstrate the CP phenomena along the membrane length. By using a model based on the modified Maxwell Stefan equation expressed as a function of volume fractions of both protein (BSA) and accompanying ions, they predicted the permeate flux, volume fractions of BSA on the membrane surface and the osmotic pressure difference over the membrane under different pH and ionic strengths in the feed solution. Haribabu et al. [18] pointed out the importance to show the non-uniformity of parameters like local transmembrane pressure, flow velocity, and concentration at different positions of the membrane in the cross-flow filtration. They advised using a multi-dimensional numerical treatment instead of a one dimensional or area-averaged models.

As will be described in detail in the next section, also our 2D-CFD model is based on common equations for conservation of mass and momentum. Namely, the modified Brinkman equations for the fluid flow and mass conservation equations for the salt and protein species containing convective, and dispersion terms. In contrast to hollow fiber modules, where the inner volume of the fibers but also the void volume of the containment housing the fibers is open space only filled by the fluid, all flow channels of our module are filled by a structured 3D-printed grid supporting the membranes on both sides (see SI Fig. S1). The grid can be looked at as an anisotropic porous structure causing a strong dispersion in tangential flow direction due to eddy diffusion effects when the fluid passes narrowing bifurcations. Because of the ability of the investigated membrane module to frequently change the flow direction through the membranes during continuous operation, the common way to account for transmembrane pressure increase over time by a resistance in series approach including integration terms was not appropriate. Instead we chose an approach coupling the required transmembrane pressure directly to the molecular concentration in the vicinity of the membranes. Such an approach is also known from ultrafiltration models considering osmotic pressure effects caused by concentration polarization (CP) at the membrane surface. However, the applied COMSOL physics for fluid flow do not consider osmotic pressures. As will be explained in more detail in section 2.3, therefore we introduced an apparent viscosity increase to couple the transmembrane pressure to concentration.

Currently our model does not account for irreversible membrane fouling, however the implementation should be straightforward adding a transient resistance to the constant membrane resistance, following e.g. the approach of Marcos et al. [22].

2 Materials and methods

2.1 SPTFF set-up and experiments for model validation

The SPTFF module used in our theoretical and experimental investigations has been introduced in detail in our previous study [17]. In brief, the module is composed of three parts, including two lateral parts through which either diafiltration buffer or permeate is flowing, and a middle part which includes the inlet of feed and the outlet of retentate (Fig. 1B). Each of the parts contains a flat flow channel having a cross-section of 2×20 mm² filled with a fine 3D-printed grid supporting the membrane and guiding the flow. Details about the grid structure can be found in section 2.3.2 and the supporting information (Fig. S4). Between the middle and the lateral part there are two membranes of the same type, both facing with their selective layer towards the middle channel. Due to size exclusion, the protein entering with the feed can only move within the channel confined by the middle part and the adjacent membranes. Each membrane has an effective area of 2972 mm² along a flow path length of 24.5 cm. For operation, the module was integrated into a FPLC Äkta system (purifier UPC 10, GE Healthcare, Uppsala, Sweden) including an additional sampling pump as well

online detectors for UV/Vis adsorption, conductivity and pH (see SI Fig. S2). The three double-piston high pressure pumps were able to adjust precise flow rates of feed, retentate and DF buffer, and thus also fixing the flow rate of the permeate due to the incompressibility of the fluids. Therefore, in contrast to common UF systems having pressure dependent permeate fluxes, our set-up controls the fluxes while the pressures in the different parts of the module result from the transient permeabilities. The system was operated in plain diafiltration mode, saying the feed and effluent flow rates always were kept identical as 0.25 or 0.5 ml/min (corresponding to fluxes of 5.0 or 10.1 LMH). In the experiments for model validation, a constant diavolume of 7.2 was conducted, corresponding to a DF buffer flow rate of 1.8 and 3.6 ml/min. The maximum transmembrane pressures observed in those experiments were in the range of 0.55 to 1.98 bar. As a consequence, also the permeate flow rate directly corresponded to the flow rate of the DF buffer. In addition, the multiport valves of the FPLC system allowed an easy switching of the perfusion directions through the membranes, as illustrated in Fig. 1B. Finally, the pressure in the diafiltration inlet was recorded by an external pressure sensor.

For the experiments conducted to validate the model predictions, the model protein bovine serum albumin (BSA, 67 kDa, PanReac AppliChem, Darmstadt, Germany) was used. A mixture of 100 mM sodium chloride and 30 mM mono-sodium phosphate buffer at pH 7.10 (Merck KGaA, Darmstadt, Germany) was used as carrier phase for the BSA in the feed solution. The ultrapure water used to exchange the feed buffer and all ultrapure water used in the experiments was prepared by a Sartorius arium® pro system (Sartorius, Göttingen, Germany). The polyethersulfone (PSE) 30 kDa cutoff membrane manufactured by Pall Life Sciences (Hauppauge, USA) was mounted in the 3D-printed membrane module for continuous DF. The experiments were conducted with constant feed flow rates of 0.25 or 0.5 ml/min (corresponding 5.0 or 10.1 LMH when referred to the membrane area). In addition, a constant flow rate of DF buffer of 1.8 or 3.6 ml/min was pumped into the lateral part of the module, resulting in a fixed number of 7.2 diavolumes. This DF buffer flow had to pass both membranes resulting in a specific membrane flux of 36 or 72 LMH. Depending on the switching intervals of DF buffer flow direction, the maximum transmembrane pressures detected in those experiments were in the range of 0.55 to 1.98 bar.

2.2 Analytical methods

In the effluent of the retentate, the concentrations of BSA and salt were measured and recorded online using a UV/Vis sensor at the absorbance wavelength of 280 nm and a conductivity meter, respectively. Two key parameters were calculated to evaluate the system with respect to transient protein accumulation and diafiltration performance: concentration factor (CF) and diafiltration efficiency (DE). The factor CF was defined as the ratio of concentration of BSA in the retentate and the feed:

$$CF = \frac{c_{BSA,R}}{c_{BSA,F}} \tag{1}$$

Since the retentate and feed flow had the same flow rates in all experiments, the idealized value of CF always has been equal to one, assuming no built-up of concentration polarization occurring during the filtration process. The factor DE was calculated based on the equation (2).

$$DE\ (\%) = \left(1 - \frac{c_{salt,R}}{c_{salt,F}}\right) \times 100\% \tag{2}$$

Where $c_{salt,R}$ and $c_{salt,F}$ are the concentrations of salt in the retentate and feed solution, respectively.

2.3 Modelling

2.3.1 Governing equations for fluid dynamics

The modified Brinkman equations were used to compute fluid velocity and pressure fields within the porous grid structure of the module parts as well as within the membranes. The modified Brinkman equation extends Darcy's law to describe the dissipation of the kinetic energy by viscous shear, similar to the Navier-Stokes equations. Depending on the intensity of this shear, the resulting flow patterns are located between pure plug flow in a porous structure with small pores and the laminar flow profile of an open channel. The modified Brinkman equations can be written as [26]:

$$\nabla p = -\frac{\mu}{\kappa}\boldsymbol{u} + \frac{\mu}{\varepsilon}\nabla^2\boldsymbol{u} - \frac{\rho}{\varepsilon}\frac{\partial \boldsymbol{u}}{\partial t} \tag{3}$$

With κ being the intrinsic permeability of the porous media permeated by the fluid and μ is the apparent viscosity of the fluid (the derivation of this equation is given in the SI part S13). The first term on the right side represents the common Darcy equation while the second one was added by Brinkman. An important feature of the introduction of the second term is, that it allows satisfying a no-slip condition when the porous media is confined by a solid wall. In addition, it also enables the formulation of a "self-consistent" set of equations when a volume is only partly filled by a porous media and the other part is e.g. an open channel in which laminar flow conditions prevail. Looking at eq. (3), the use of a single value of the permeability of the porous media is somewhat contradictory to the statement that the 3D-printed grid has an anisotropic structure. However, the anisotropy is between the tangential flow direction and the direction perpendicular to it. Therefore, permeability within tangential flow direction can be considered as homogenous, and in the perpendicular direction the flow is governed by the membrane permeability, while the one of the grid can be neglected. In order to calculate the flow and pressure profiles the equation describing the conservation of mass for an incompressible fluid with constant density is required in addition:

$$\nabla \boldsymbol{u} = 0 \tag{4}$$

For the estimation of the intrinsic permeability of the porous grid structure, the Kozeny-Carman equation using a porosity of $\varepsilon_g = 0.6$ and a characteristic length $L_g = 1$ mm is used.

$$\kappa_g = \frac{L_g^2 \cdot \varepsilon_g^3}{180 \left(1 - \varepsilon_g\right)^2} \tag{5}$$

The intrinsic permeability of the membranes κ_m could be calculated from the hydraulic tests of the membrane with pure water:

$$\kappa_m = \frac{Q \cdot \mu \cdot d_m}{TMP \cdot A} \tag{6}$$

where Q is the flow rate, d_m is the thickness of the membrane, TMP is the transmembrane pressure, and A is the membrane area. With respect to the boundary conditions, our model specifies the volume flows with fully developed flow profile in all four inlets and outlets, instead of the common specification of a fixed pressure in the retentate and permeate outlet. The first reason for this choice is given by the fact that we operate the system at fixed volume flows by the help of the double piston pumps of the setup, independent of the occurring pressures. The second reason results from the possibility to easily implement the change of the perfusion direction through the membrane this way. For switching the flow direction, the inlet of DF buffer changes its position and at the same time the former inlet is closed by a valve (see Fig. 1B). The same holds for the former and new position of the permeate outlet. In our model this switching can simply be achieved by a periodic rectangle function controlling the flows in the in- and outlets. However, as can be expected, the control of all in- and outlets of a closed compartment in combination with the assumption of an incompressible fluid unavoidable leads to numerical problems. Because of the assumption of incompressibility even very tiny differences in the sums of in- and outlet flows would result in physically senseless pressures and aborting of the program. Therefore, as will be explained in more detail in the SI Fig. S3, we introduced an additional artificial outlet in the model, which however, has only a very low permeability. The boundary condition is set in a way that the outlet is at ambient pressure. Because of the low permeability the flux in this outlet is completely negligible in the mass balance and the flow profiles, nevertheless it prevents that the model is overdetermined and allows the calculation of meaningful transmembrane pressures.

2.3.2 Governing equations for the transport of dissolved species

Mass transfer of both, BSA and salt, is simulated by the 'transport of diluted species' physics of COMSOL. Convective flux as well as dispersive flux caused by diffusion due to concentration gradients and eddy dispersion are the contributors to species transport. Accordingly, the mass balance accounting for species accumulation and transport is given as:

$$\frac{\partial(\varepsilon c_i)}{\partial t} + \nabla \cdot \boldsymbol{J_i} + \boldsymbol{u} \cdot \nabla c_i = 0 \tag{7}$$

where $\boldsymbol{J_i}$ is the effective dispersive flux vector given by eq. (8).

$$\boldsymbol{J_i} = -(\boldsymbol{D_{D,i}} + D_{e,i})\nabla c_i \tag{8}$$

In eq. (8) $\boldsymbol{D_{D,i}}$ and $D_{e,i}$ are the dispersion tensor and the effective diffusivity, respectively. The effective diffusivities of the species in the grid structure are related to the diffusivities in free solution by:

$$D_{e,i} = \frac{\varepsilon}{\tau} D_{F,i} \qquad (9)$$

where τ is the tortuosity and $D_{F,i}$ is the binary diffusion coefficient of the species in water. For the tortuosity the correlation of Millington & Quirk for an ideal porous material is used [27]:

$$\tau = \varepsilon^{-1/3} \qquad (10)$$

For the dispersion tensor a simplified form is used, which only contains the terms $D_{D,x}$ and $D_{D,y}$ of the main diagonal. As can be seen in Table 1 the used values for these two terms differ strongly. While this would be rather unusual for common porous media encountered in biotechnology, such as e.g. a chromatography bed or a monolith, one has to keep in mind that our structured 3D-printed grid is highly anisotropic. In x-direction, the flow has to pass about 80 cube shaped chambers of $3 \times 3 \times 2$ mm^3 with only a narrow window of about 1×1 mm^2 in the walls between the chambers. Such an arrangement results in strongly varying path lengths of different streamlines and therefore strong eddy diffusion effects in x-direction with a characteristic structure dimension of about 1mm. The situation is completely different if one looks at the flow path in y-direction. In y-direction the grid forms short, completely open quadratic channels, without any obstacles for the flow (see SI Fig. S4). Another reason for the large difference between $D_{D,x}$ and $D_{D,y}$ is that the mean interstitial flow velocity in x-direction is more than 100-times larger than the mean interstitial flow velocity in y-direction. A rough estimation of the dispersion coefficient in tangential flow direction $D_{D,x}$ can be obtained by the correlation of Rastegar and Gu for axial dispersion in packed bed column [28,29].

$$D_{ax} = \frac{d_p \cdot u_{int} \cdot \varepsilon}{0.2 + 0.011 \cdot (\varepsilon \cdot Re_p)^{0.48}} \qquad (11)$$

Replacing the particle diameter by the diameter of repetitive cubes and using a typical values of $u_{int} = 4.63 \cdot 10^{-4}$ m/s ($\varepsilon = 0.6$), corresponding to the velocity in the middle channel in case of a feed flow rate of 0.5 ml/min, one obtains a dispersive coefficient of $4 \cdot 10^{-6}$ m^2/s. Fitting our model to the experimental results we determined a three times higher $D_{D,x}$ value of $1.2 \cdot 10^{-5}$ m^2/s. On the one hand this shows, that the correlation of Rastegar gives an estimate in the correct magnitude, on the other hand it becomes obvious that the flow around spherical beads is only a very rough approximation of the flow patterns within our grid.

In case of low Reynolds numbers (Re < 10), as they prevail in our setup, eq. (11) predicts an almost linear dependence between the dispersion coefficient and the flow velocity. Therefore, the dispersion coefficients at different flow rates can easily be extrapolated from the value determined at $Q_{F,0} = 0.5$ ml/min by a factor

$f = Q/Q_{F,0} = u/u_{int,0}$. The molecular diffusion and dispersion coefficients applied in the simulations are summarized in Table 1.

Table 1: Molecular diffusion and dispersion coefficients in the grid structure[*]

	$i=$ BSA	$i=$ salt
$D_{F,i}$ (m²/s)	$5 \cdot 10^{-11}$	$1.5 \cdot 10^{-9}$
$D_{D,i,x}$ (m²/s)	$1.2 \cdot 10^{-5} \cdot f$	$1.2 \cdot 10^{-5} \cdot f$
$D_{D,i,y}$ (m²/s)	$2 \cdot 10^{-9} \cdot f$	$2 \cdot 10^{-9} \cdot f$

[*] calculated for $Q_{F,0} = 0.5$ ml/min

In case of BSA, we assume that the molecule is completely retained by the membrane while the fluid can permeate. As a result, the phenomenon of concentration polarization occurs, meaning BSA accumulates in the vicinity of the membrane and the local concentration strongly increase. This happens until an equilibrium is reached in which the diffusive flux back into the bulk solution matches the convective flux transporting BSA towards the membrane. The phenomenon of concentration polarization is accompanied by the requirement of an increased transmembrane pressure in order to keep the flow through the membrane constant. As mentioned in the introduction, we do not use the more common resistance in series approach to consider this effect, but we simulate the increased flow resistance by means of an apparent viscosity increase in a region which stretches 150 µm above the membrane. Within this region the apparent viscosity is not a constant but a function of the local BSA concentration (see section 3.2.2). Because of the fact that we model all our flows as flow through a porous grid (eq. 3), the increased viscosity automatically results in an increased flow resistance and increased transmembrane pressures. By this approach the flow resistance can dynamically follow the local BSA concentration close to the membrane. This concentration increases due to accumulation during normal operation but also abruptly drops when the flow direction through the membrane is switched.

3 Results and discussion

3.1 Hydrodynamics characterization

For the investigation of the plain hydrodynamic behavior of the module, in the beginning, idealized experiments without the presence of BSA were conducted. In this case, solely a buffer exchange between the salt in the feed flow and pure water, serving as DF buffer, took place.

3.1.1 Simulation of the dynamic salt profiles

To explore the influence of periodic switching of the flow direction of DF buffer in single-pass counter-current diafiltration, a representative simulation applying a salt concentration of $c_{F,salt} = 100$ mol/m³ at a feed flow rate of $Q_F = 0.25$ ml/min was conducted. Fig. 2 displays the simulated transport of salt in the module while alternating the flow direction of DF buffer every 180 s. The chosen value of 7.2 diavolumes results in a degree of buffer exchange of around 95%. As can be seen for the concentration contour at 170 s the DF buffer flowing from the top lateral part of the module to the bottom one shifts the salt downwards to the lower membrane during the first interval. The DF buffer enters at the upper right inlet and leaves the module at the lower left outlet (see also Fig. 1B). So, the overall flow direction of the DF buffer is from right to left, however, during the passage of the middle part of the module, the flow direction from top to bottom is superimposed by the flow of the feed respectively retentate from left to right.
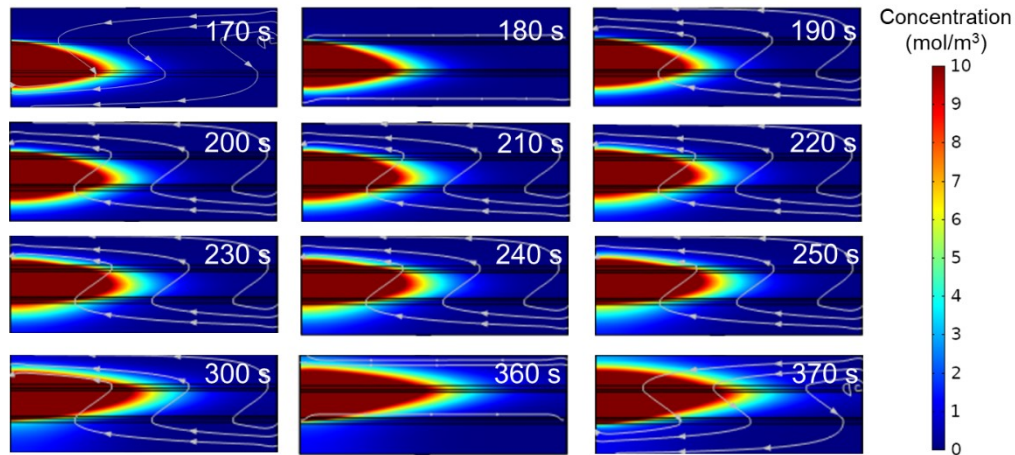

Fig. 2. Representative salt concentration profiles in the module before and after switching the flow direction of DF buffer. Parameter settings of the simulation: $c_{F,salt} = 100$ mol/m³, $Q_{DF} = 1.8$ ml/min, $Q_F = 0.25$ ml/min and $t_S = 180$ s. The color legend of the contour plot of the salt concentration is restricted to the range between 0 and 10 mol/m³ in order to give a better picture of the spatial distribution of the lower salt concentrations dominating at the investigated degrees of buffer exchange. In addition to the contour plot streamlines of the flow profile in the module are plotted to illustrate the abruptly changing flow pattern at the switching events.

Therefore, the streamlines show a kind of zig-zag profile. At the switching times there is a very short transition period in which the flow direction of the DF-buffer changes in a way that it now enters at the lower right inlet and leaves at the upper left outlet. By this, the DF buffer flow through the membranes changes its direction, however, the overall flow direction of the DF buffer is still countercurrent to the direction of the feed flow. Mainly because of the convection of the DF buffer across the membrane, but partly also because of diffusion effects caused by the concentration difference of salt between the middle

and the lateral parts, most of the salt entering with the feed stream is transported into the upper lateral part of the module in the period between 180 and 360 s. Note that while penetrating the upper membrane and entering the upper lateral part, the majority of the salt stays in the vicinity of the membrane while flowing towards the effluent. This is because the flow in x-direction is strongly dominating in the lateral parts and there is only little mixing of the fluid compartments in y-direction. While this characteristic is of minor significance in a non-alternating operation mode, it reduces the efficiency if the flow direction through the membrane is switched periodically. Changing the flow direction will transport fluid compartments containing high salt loads back from the lateral part into the middle part. This behavior can be observed e.g. by looking at the stream lines in the lower lateral part in the plots between 190 s and approx. 250 s. About 120 s after the switching event at 180 s (corresponding to the plot at 300 s) the salt in the lower lateral part is mainly flushed away by fresh DF buffer entering this part. However, at 360 s the next switch of the flow direction is initiated, now transporting salt from the upper lateral part back into the middle part (see the plot at 370 s). Therefore, each switching event causes a reduction of the buffer exchange efficiency lasting for a certain time. If the period between the switching events is long enough, this temporary disturbance does not interfere too much the overall performance. However, according to the simulation, for short switching intervals a severe reduction of the buffer exchange performance can be expected. Besides, the concentration of salt detected in the retentate shows a wave-like trend due to the periodic switching of the flow direction of DF buffer (see in SI Fig. S4). There may be cases of continuous downstream processing where even such short fluctuations are unwanted. However, integrating a small mixing vessel in the effluent having an average residence time in the range of 2-3 switching periods could easily solve this problem.

3.1.2 Model validation

As discussed above, the model predicts an increasing reduction of the buffer exchange performance, when the period between the switching events gets shorter. In this section, this forecast is compared to experimental data, in order to see if the developed model is able to satisfyingly predict the relationship quantitatively. For this, a series of experiments with two feed flow rates and varying switching intervals between 100 and 600 s were conducted. As in the case of the idealized simulation, the experiments were run with plain buffers without the presence of BSA.
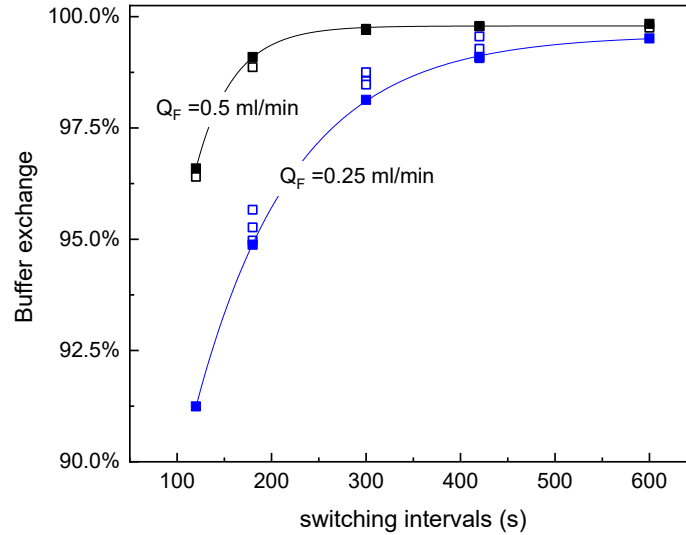
Fig. 3. Achieved degrees of buffer exchange in single pass countercurrent diafiltration experiments with periodic switching of the flow direction of DF buffer through the membranes. The figure shows the experimentally obtained and simulated degrees for two different feed flow rates Q_F and various values of the switching interval of the DF buffer direction. The flow rate of the DF buffer was adjusted to the Q_F in order to achieve a constant diavolume of 7.2. Higher Q_F and longer switching intervals result in a better buffer exchange performance. Open symbol: experimental value, filled symbol: simulated value.

As shown in Fig. 3, with increasing switching intervals and volumetric feed flow rate, both modeling and experimental results show in good agreement that the buffer exchange efficiency increased. As shown in the previous section, after each switching event there follows a period in which a part of the salt already transported into the permeate in the lateral part of the module is pushed back into the middle part of the module. In case of longer switching intervals the fraction of this period in relation to the total interval is not large and therefore the disturbing influence is low. With increasing switching intervals, the buffer exchange efficiency reaches a plateau value corresponding to the buffer exchange efficiency of unidirectional operation at the same amount of diavolumes. The dependence of the buffer exchange efficiency on the feed flow rate seems to be counter-intuitive on first sight. Assuming the same flow patterns in case of a constant ratio between Q_{DF} and Q_F (same diavolumes) one could expect a constant degree of buffer exchange, despite the higher absolute flow rates. However, the experimental as well as the simulation results show a clearly improved efficiency if higher flow rates are applied at the same switching intervals. The explanation for this behavior can be found in the fact that a higher Q_{DF} shortens the period which is required to flush out residual salt in the lateral part after switching. In first approximation it can be assumed that doubling Q_{DF} will cut the time approximately in half. If this assumption holds, the buffer exchange efficiency of an experiment $Q_F = 0.25$ ml/min and 400 s switching interval should be the same than in case of $Q_F = 0.5$ ml/min and 200 s. As can be seen in Figure 3, this is nearly the case, in the simulation as well as in the

experiment. Overall, the comparison between the experimental and simulated data shows that the developed FEM model is able to reliably predict the hydrodynamic behavior of our diafiltration module in case the dissolved substances are able to freely pass the membranes. In the next section, the model will be extended to the case that the feed also contains macromolecules being retained by the membranes.

3.2 Concentration polarization and pressure build-up

In the above section it was shown, that in the absence of any retained macromolecules and under the assumption of a constant number of diavolumes applied, increasing feed flow rates would result in increasing buffer exchange efficiencies for a given switching interval of the flow direction of DF buffer. However, in the presence of macromolecules such as BSA, the applicable feed and DF buffer flows are limited by the maximum pressure the diafiltration module can tolerate. Therefore, a realistic model of the device must be able to predict the effects of concentration polarization of retained macromolecules, especially the resulting pressure build-up.

3.2.1 Simulated time course of BSA concentration within the module

Fig. 4 shows the simulated time course of the BSA concentration profiles, again in the period between 170 s and 370 s for an experiment having a switching interval of 180 s. Because our model assumes a complete retention of BSA by the membranes, BSA concentration profiles only differ from zero in the middle part of the module. The single plots show snapshots of the contour of the BSA concentration for t = 170 s, 180 s, … 370 s. Consequently, the plots show the contour shortly before the first switching event and for the time period between the first and the second switching event. During these times, the operation of the module has not reached a quasi-stationary state and the plots show the situation when the BSA concentration profiles propagate through the module. Comparable plots of BSA concentration contours in quasi-stationary operation can be found in the SI Fig. S5. In the plot at 170 s it can be seen that the DF buffer flow pointing from the upper lateral part of the module towards the lower lateral part pushes BSA towards the lower membrane in the inlet region of the middle part. However, in contrast to the behavior of salt discussed in Fig. 3, BSA cannot penetrate the UF membrane. Therefore, a rapid accumulation of BSA and a corresponding concentration polarization is predicted by the model (details see in SI Fig. S6). In case of constant operation conditions with unidirectional flow of DF buffer through the membranes, the concentrated BSA layer would slowly propagate through the module until its end reaches the effluent of the middle part and a stationary state is reached.
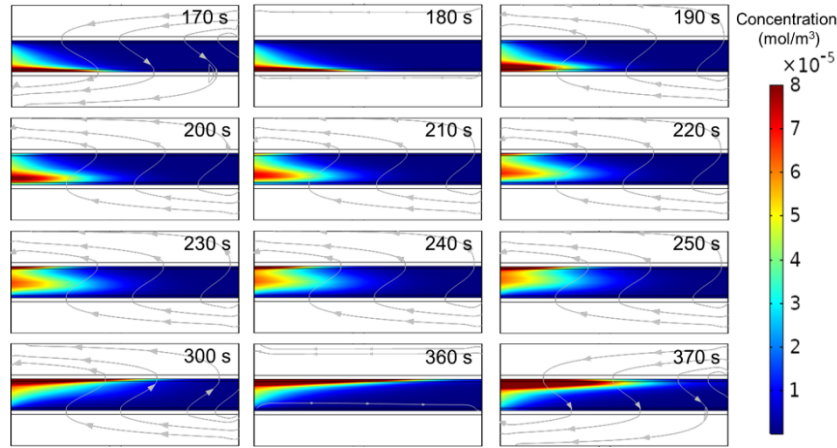
Fig. 4. Representative protein BSA concentration profiles in the module before and after switching the flow direction of DF buffer applying BSA ($c_{F, BSA} = 5$ g/L) and salt ($c_{F, salt} = 100$ mol/m³) in the feed stream. The modeling is simulated under the identical parameter settings as in section 3.1.1. The colorful surface and gray streamline represent the BSA concentration distribution and flow direction, respectively.

However, in the presented case, the direction of DF buffer flow is abruptly changed at 180 s. In the following snapshots taken at 10 s intervals it shows that the accumulated BSA layer detaches from the lower membrane and, driven by the vertical component of the DF buffer flow, slowly moves towards the upper membrane. In addition, while passing the central region of the module, the liquid compartments with highly concentrated BSA are also moved in positive x-direction towards the effluent of the middle part. Finally, because of dispersion effects, the concentrated region also starts to blur. However, when the 'bubble' of concentrated BSA hits the upper membrane the accumulation and concentration polarization quickly restore and about 120 s after the switching a new, almost stationary concentration profile is obtained which slowly propagates towards the effluent. It is obvious, that the duration of the intermediate state, represented by the concentrated bubble moving vertically through the module, depends on the flow rate of DF buffer. Looking at the progression of the simulated pressure in the middle part of the module during the operation phase it shows that the formation of an accumulation layer of BSA is accompanied by a rapid increase of the pressure (Fig. S7). However, each switching event results in an almost instantaneous drop of the pressure towards the level caused by the flux of pure DF buffer through the membrane. In the following interval, the pressure recovers because of the renewed BSA accumulation on the opposite membrane until the increase is stopped by a new switching event. If switching is omitted, the pressure increases up to a plateau value (see Fig. S8). This situation corresponds with a stationary accumulation and concentration polarization profile in the module. In case of a conventional 'constant pressure' operation of an UF module, the formation of a highly concentrated accumulation layer at the membrane decreases the permeate flux through the membrane. However, in the developed system all flow rates are kept constant by the application of high-

pressure double piston pumps guaranteeing a constant flow also in case of increased back pressures. After a switching event, the concentrated BSA is pushed back into the retentate and subsequently a part of it builds up on the opposite membrane while the other part appears in the effluent of the retentate. This explains the wave-like trend of the effluent concentration of BSA observed in the experiments (see Fig. S6 and the respective graphs in [17]).

3.2.2 Model validation

All simulations were conducted applying pure diafiltration, saying the retentate flow rate was exactly matching the feed flow rate, resulting in the average concentration of BSA in the effluent being the same than the one in the feed, when the system reaches its quasi-stationary state. Therefore, for validation it is more useful to compare the simulated and experimental results of the maximum pressure built-up caused by the accumulated BSA. The maximum pressure occurring during quasi-stationary operation is also of high practical interest, because in order to guarantee a reliable operation of our 3D-printed diafiltration system, the pressures in all parts of the module must not exceed a pressure limit of 3 bar. This limitation is comparable to the recommended pressure limits of many UF processes for proteins, because transmembrane pressures above 2 - 3 bar normally do not result in higher permeate fluxes [1,13,30]. When investigating the observed pressures, the special structure of our system with two membranes must be taken into account. Assuming the flow direction of DF buffer from top to bottom, the different pressures in the module can be defined as illustrated in Fig. 5 [1].
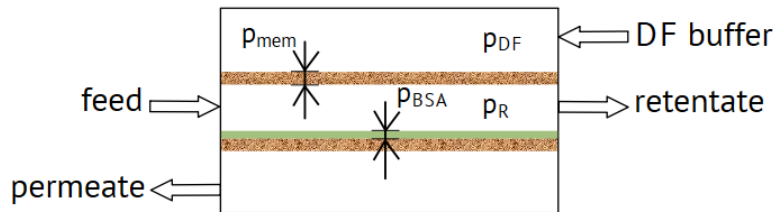

Fig. 5. Schematic of pressures in each part of the module. For a given flux of DF buffer the pressure drop of the membrane p_{mem} is a constant value determined by the intrinsic properties of membrane.

Soon after the accumulation layer starts to form, the pressure in the middle part is mainly related to the concentrated BSA at the membrane surface. In addition, the pressure drops caused by the permeate passing the lower membrane adds to the total transmembrane pressure between the middle and the lower lateral part of the module. In contrast, the transmembrane pressure between the upper lateral part and the middle part is only caused by the DF buffer passing the upper membrane. Because the upper and lower membranes are

---

[1] As it is common praxis, we us the expression 'pressure' in the sense of pressure difference against the ambient pressure of 1 bar. Because there is no restrictor valve in the permeate effluent, the pressure in this part of the module is assumed to be zero and the TMP of the lower membrane reduces to P_R.

identical and the additional salt in the permeate does not have a significant influence on the permeability, the pressure drop of the membrane itself (p_{mem}) is the same for both membranes. Therefore, the transmembrane pressures can be calculated by eq. (12) and (13).

$$TMP_{upper} = p_{mem} = p_{DF} - p_R \qquad (12)$$

$$TMP_{lower} = p_R = p_{BSA} + p_{mem} \qquad (13)$$

By substituting eq. (13) into equation (12) one obtains:

$$p_{DF} = p_{BSA} + 2 \times p_{mem} \qquad (14)$$

This shows that the pressure required to pump the DF buffer into the module is defining the maximum load onto the 3D-printed material and therefore is used for the comparison. Fig. 6 shows the maximum experimental and simulated values of p_{DF} for two different feed flow rates and various switching intervals. All experiments and simulations were conducted at a constant value of 7.2 diavolumes and a concentration of BSA in the feed of 5 g/L. While for the higher flow rates the simulated pressures reach up to more than 7 bar, the experimental data had to be restricted to values slightly higher than the mentioned limit of 3 bar. As can be expected, higher feed flow rates but also longer switching intervals result in higher values of $p_{DF,max}$. The slope of the increase of $p_{DF,max}$ is steeper in case of $Q_F = 0.5$ ml/min (10.1 LMH) than in case of 0.25 ml/min (5.05 LMH). However, looking e.g. at the relative difference of $p_{DF,max}$ between $t_S = 200$ s and 400 s, it shows that both curves increased by about the same factor of two. As explained in the theoretical section, we simulate the pressure increase resulting from concentration polarization by the help of an apparent viscosity increase of the fluid in the accumulation layer at the membrane surface. In order to obtain a quantitative prediction of the pressure, the relation between this apparent viscosity increase and the BSA concentration had to be fitted once. However, thereafter all simulated results have been obtained with the following correlation:

$$\mu_{apparent} = 1 \cdot 10^{-3} Pa \cdot s + 3.39 \cdot 10^{7} Pa \cdot s \times (\frac{c_{BSA}}{c_{BSA,max}})^2 \qquad (15)$$

The parameter $c_{BSA,max}$ was set to 6.9 mol/m^3 (460 g/L), which was reported to be the gelling point of BSA [21]. At this point it is important to clearly state that the apparent viscosity has no physical meaning, but solely serves to couple the pressure increase to concentration polarization. Calculating osmotic pressures differences across the membranes would be a more physically sound approach, however, as mentioned in the introduction, the applied hydrodynamics model does not offer this possibility. We thoroughly checked the implications of the introduction of the apparent viscosity besides the intended pressure increase. In the initial phase of the simulation, regions close to the feed inlet show BSA accumulation already, while the BSA front has not reached regions close to the retentate outlet. In consequence, the increased flow resistance at the inlet regions results in an inhomogeneous permeate flux through the membrane. However, when the

BSA front has reached the outlet, the flow resistance above the membrane equalizes and the permeate flux is practically the same at different parts of the module. In this stationary state, the laminar flow profile is independent of the correlation used for the apparent viscosity.

In conclusion, after fitting once the correlation for apparent viscosity, our model was able to predict the dependence of the dynamic pressure built-up onto different operation parameters to a satisfying degree, as can been seen by a comparison of the simulated (filled cycles) and experimental (open cycles) values in Fig 6. Note that $p_{DF,max}$ was lower than the allowed pressure limit for all tested switching intervals at $Q_F =$ 0.25 ml/min. When doubling Q_F to 0.5 ml/min the simulated values of $p_{DF,max}$ reached up to more than 7 bar for $t_S = 600$ s, however, when choosing a switching interval of around 180 s, the exceeding of the pressure limit could be avoided. This shows, that on the one hand, the new operation mode with alternating direction of the DF buffer flow through the membranes allows to operate the system at feed flow rates which, without switching, would quickly exceed the allowed pressure limits. On the other hand, as seen in Fig. 3 short switching intervals clearly deteriorate the achievable diafiltration efficiency. The question if there exists an optimum set of Q_F and t_S-values will be investigated more deeply in section 3.3.2.
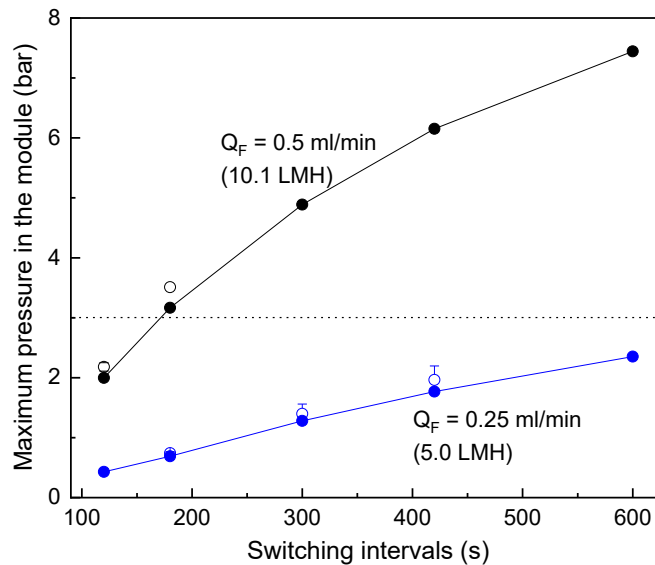

Fig. 6. Effect of the duration of the switching interval for on the maximum pressure built-up in the developed diafiltration module. $c_{F,BSA} = 7.52 \cdot 10^{-3}$ mol/m³ (5 g/L), DV = 7.2, $Q_F = 0.25$ ml/min and 0.5 ml/min, respectively. The dotted line at $p_{DF,max} = 3$ bar marks the pressure limit of the module. Open symbols: experimental values, filled symbols: simulated values. Error bars are equal to ± standard deviation, the error bar for switching interval 180 s at $Q_F = 0.25$ ml/min is within the size of the symbol.

3.3 Model based parameter screening

3.3.1 Unidirectional DF buffer flow

From the data presented in Fig. 3 it became obvious that the highest degrees of buffer exchange are obtained for the longest switching intervals. Consequently, it is worth to investigate the case with no switching events, synonymous to infinitely long switching intervals, in more detail. As shown in Fig. 6, long switching intervals in combination with the presence of BSA in the feed stream can quickly lead to the pressure limit being exceeded. Therefore, it is interesting to screen for parameter combinations Q_F, $c_{F,BSA}$, DV at which the final maximum pressure $p_{DF,max}$, obtained without switching the flow direction of the DF buffer, just approaches the allowed pressure limit. In order to speed-up this screening process, we extracted a semi-empirical correlation from the complete set of experimental data (see SI Fig. S11). The multi-parameter correlation describes a relation between the maximum pressure $p_{DF,max}$ and the parameters $c_{F,BSA}$, Q_F, Q_{DF}, as well as t_S. Evaluating this correlation for $t_S \rightarrow \infty$ allows to quickly find suitable starting parameters for the precise screening using the COMSOL model.
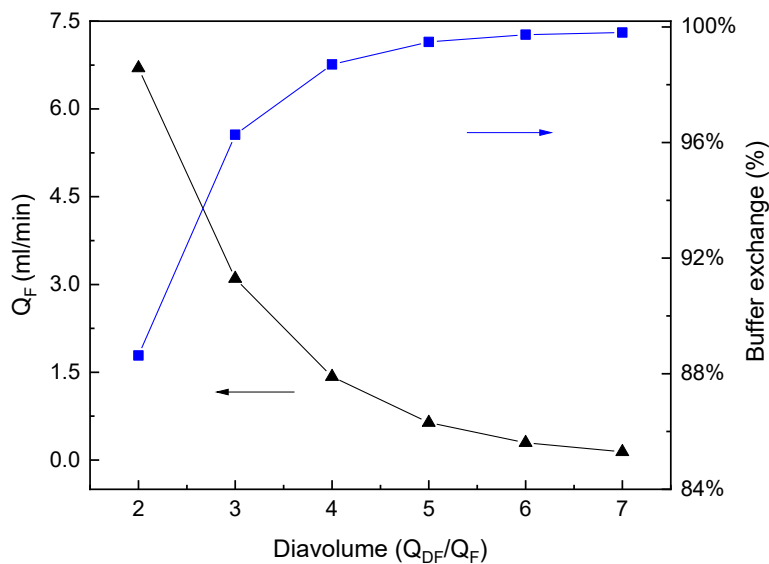

Fig. 7. Effect of the used amount of diavolumes on the maximum feed flow rate Q_F applicable without exceeding the pressure limit of $p_{DF,max}$ = 3 bar. On the right y-axis the corresponding degree of buffer exchange is plotted. The simulated feed solution contains 5 g/L BSA and 100 mol/m³ salt.

As mentioned, the boundary conditions of this first parameter study were to find parameter combinations Q_F, DV which approach the pressure limit of 3 bar when applying the non-switching diafiltration mode (see Fig. 7). There are two ways to interpret the presented curves. First, one can start with a given feed flux at the left y-axis. Then the black line with the filled triangles will give the maximum number of diavolumes, corresponding with the maximum applicable Q_{DF}, which is allowed without exceeding the pressure limit. In case of Q_F = 1.5 ml/min this number is approx. four diavolumes. Knowing DV the blue line together

with the right y-axis will tell the degree of buffer exchange which can be expected for our module and the given feed concentration of BSA. In our example, this would be a buffer exchange of approx. 98.5%. The second way to interpret the Figure is to start with a desired buffer exchange efficiency on the right y-axis. The blue line then tells the required amount of diavolumes, and with this the black line in combination with the left y-axis shows the maximum Q_F possible. For example, a requested buffer exchange of 96% requires approx. 3 diavolumes, and allows a maximum Q_F of approx. 3 ml/min. When the applied Q_F is lower than this maximum Q_F, the resulting final pressure will be lower than the pressure limit (see Fig. S8).

3.3.2 Switching flow direction of DF buffer

Fig. 6 shows that by introducing an alternating flow direction of the DF buffer, the maximum pressure built-up in the module can be restricted. The shorter the intervals between the switching events, the lower is the maximum pressure obtained during operation. Therefore, for a given Q_F the application of an alternating DF buffer direction will allow to apply higher values of Q_{DF} than in the case of unidirectional DF buffer flow, without exceed the pressure limit. Higher ratios of Q_{DF}/Q_F correspond to a higher number of diavolumes. Therefore, on the one hand one could expect that the application of the switching mode will enable to reach higher diafiltration efficiencies for a given Q_F, while staying within the given pressure limits. On the other hand, Fig. 3 clearly shows the negative influence of frequent switches of the DF buffer direction onto the diafiltration efficiency. In order to answer the question if these opposing effects will result in an optimum switching interval with optimal diafiltration efficiency we extended our parameter study to cases with various Q_F, DV, and t_S values. Fig. 8A indicates the switching interval required in order to obtain a certain number of diavolumes (DV) for a given feed flow rate Q_F without exceed the pressure limit. In order to allow comparability to other UF/DF modules, we plotted the feed flux, saying the feed flow rates related to the effective membrane area, of our module on the x-axis, with an absolute Q_F value of 0.5 ml/min corresponding to Q_F/A = 10.1 LMH. The vertical lines mark the Q_F/A values below which no switching is required for a certain DV. E.g. in case of a requested DV of 5, no switching is required if Q_F/A values below 13 LMH are applied. However, if this value is exceeded, the blue line indicates the switching intervals that must be applied to guarantee that the pressure limit is not surpassed. Therefore, in case of 20 LMH and DV = 5 a switching interval of approx. 180 s is required. Looking at the feed flux numbers one has to be aware, that in the case of our module the feed flux is decoupled from the permeate flux which physically flows through the membrane. In conventional diafiltration, the permeate flux is only a fraction of the feed flux, getting close to one in its maximum. In contrast, in the presented diafiltration module, the permeate flux is related to the independently applied flow rate of DF buffer. For example, in case of DV = 5, the permeate flux which has to penetrate the membrane is five times the feed flux Q_F/A.
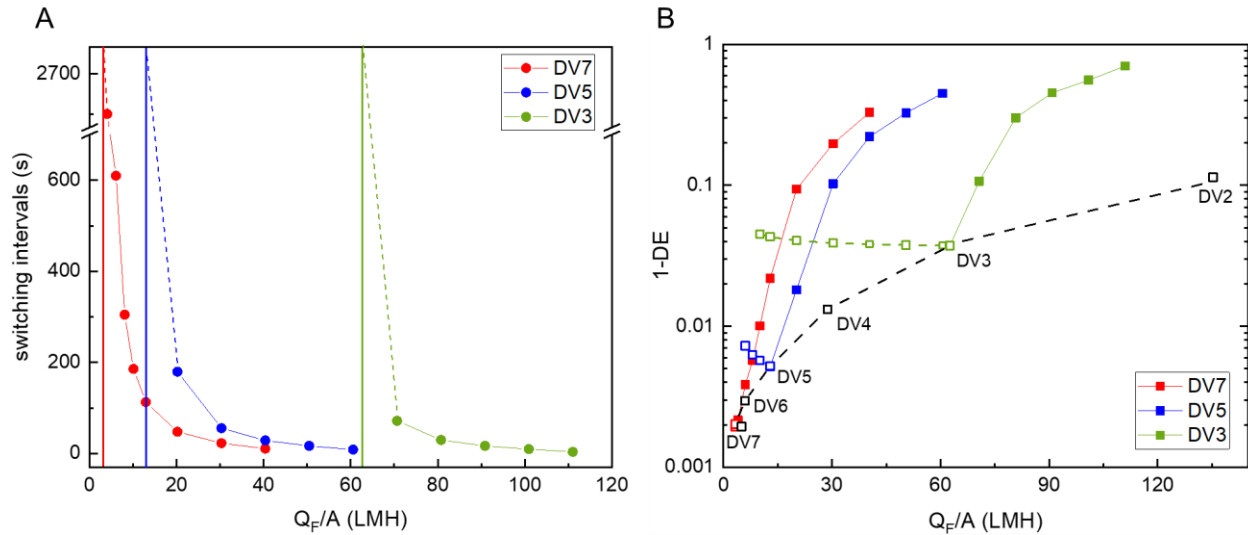
Fig. 8 A. Required switching intervals in dependence of the applied feed flux (Q_F/A) and the number of diavolumes. When the feed flux is lower than the vertical line, the operating mode changes from switching to unidirectional DF buffer flow; B. Simulated buffer exchange efficiency applying various feed fluxes, switching intervals, diavolumes and operation modes. In all cases the concentration of BSA in the feed stream was fixed at 5 g/L. The filled symbols correspond to the operation mode with switching direction of the DF buffer flow, the open symbols correspond to the operation mode with unidirectional DF buffer flow.

The stated feed flux therefore corresponds to the amount of original feed solution which can be treated by the module per time, while the physical flux impinged to the membrane is several times higher. Fig. 8B shows the predicted diafiltration efficiencies (DE) for multiple simulation runs with constant $c_{F,BSA} = 5$ g/L and $p_{DF,max} = 3$ bar but various parameter sets for Q_F, DV and t_S. In order to get a detailed picture of the system behavior at high diafiltration efficiencies, the values of 1-DE are plotted in a logarithmic scale on the y-axis. This value can also be looked at as the fraction of the original buffer in the feed remaining in the retentate. Therefore, low numbers of 1-DE are equivalent to high diafiltration efficiencies. The black dashed line results for the limiting case of unidirectional flow of DF buffer and therefore corresponds to the blue line in Fig. 7. Starting from this boundary, the lines with fully colored square symbols show the predicted diafiltration efficiencies for decreasing switching intervals t_S but a constant number of diavolumes. In accordance to Fig. 8A, decreasing switching intervals allow higher Q_F values for a given maximum pressure. However, they also result in lower diafiltration efficiencies, corresponding to higher 1-DE values. In case of the lines for DV = 3 and DV = 5 the plot also shows the calculated 1-DE values if Q_F values smaller than the limiting value for unidirectional DF buffer flow are applied. The respective results are indicated by open squares, because the conditions of these runs differ in a way that the achieved maximum pressure is below the limiting pressure. From the calculations with unidirectional DF buffer flow it can be seen, that when keeping DV constant, a reduction of Q_F does not improve diafiltration efficiency. Instead, the obtained DE

values show a slightly decreasing trend (increasing 1-DE), which may be caused by the decreasing dispersion coefficient in y-direction. However, the question if the introduction of a periodic switch of the direction of DF buffer flow can improve DE is of higher relevance for this work. As explained, the period switch allows higher fluxes through the membranes. This can be used to increase Q_F and keep DV constant, as in case of the colored lines with filled squares, but also to keep Q_F constant and increase DV. In the Figure, keeping Q_F constant is equivalent to moving along a vertical line defined by a given Q_F value. For example, one could start at the point where the blue line meets the black dashed line (DV = 5, unidirectional DF buffer flow, $Q_F/A \approx 15$ LMH) and move vertically until the intersection with the red line for DV = 7. This means, by introducing a periodic switching of the direction of DF buffer flow, one can increase the number of applied diavolumes from 5 to 7, while keeping Q_F/A and the maximum pressure constant. However, in order to meet the red line one has to move upwards in the Figure, showing that the diafiltration efficiency decreases despite the increased number of DV. In order to obtain a better DE in case of the switching mode, the slope of a line with constant DV would have to be lower than the slope of the black dashed line. From Fig. 8B it becomes obvious that, at least in the investigated parameter range, this is never the case. Therefore, with respect to the achievable DE, unidirectional flow of the DF buffer without any switching events is the optimum way of operation.

3.3.3 Comparison to other SPTFF systems and extension to higher feed concentrations

In Fig. 9, the simulated buffer exchange efficiency of our system is compared to different designs of single pass diafiltration systems reported in the literature. These include dialysis modules [31] as well as multistage continuous countercurrent diafiltration [32]. In addition, the black dash dot line indicates the diafiltration efficiency predicted by the well-known equation of constant volume diafiltration in a conventional TFF system [33]. As shown by Tan and Franzreb [34], the same correlation between the applied diavolumes and the resulting dilution efficiency holds for the investigated module with two membranes if one assumes pure plug flow in all parts of the module and neglects the effects of dispersion. Looking at the red line in Fig. 9, displaying the results of the COMSOL simulations for the operation mode with unidirectional DF buffer flow, it shows that up to the application of approx. five diavolumes, the diafiltration efficiency is slightly better than the estimation based on the simplified assumption of pure plug flow. However, both lines follow the same linear trend in this plot using a logarithmic scale on the y-axis.
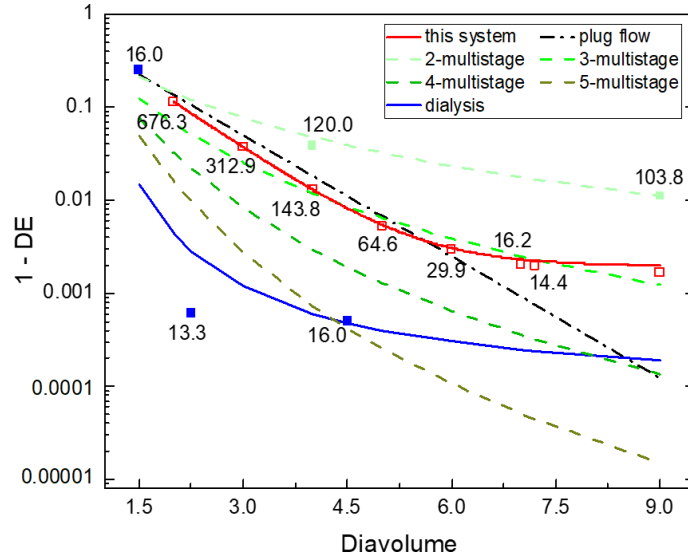
Fig. 9. Effect of the number of diavolumes applied on the achieved degree of buffer exchange for different continuous diafiltration processes. Values beside the symbols indicate the corresponding protein load per membrane area, e.g. expressed in g/(m² h). Open symbol: simulated value, filled symbol: experimental value.

At first sight, it may be surprising that the predictions of the detailed simulation of our module accounting for diffusion/dispersion effects could exceed the predicted diafiltration efficiencies of an idealized model which accounts for convective mass transport only. However, in case of a counter-current operation dispersion effects perpendicular to the flow direction can be advantageous. An impressive confirmation of this assumption is given by the blue trend line, which shows the predicted dilution efficiencies in case of pure dialysis operated in counter-current mode [31]. Although, in the used hollow-fiber dialysis module the transport of salt across the membrane is driven by diffusion only, even low numbers of diavolumes can achieve high dilution efficiencies, albeit at very low surface loads of the module. The trend that systems operated in counter-current mode can surpass the dilution efficiency of conventional constant volume diafiltration at the same number of diavolumes can also be seen for the plotted lines representing multistage continuous countercurrent diafiltration [24]. However, it requires at least three stages to match the performance of our single module or constant volume diafiltration. Beyond approx. six diavolumes all systems applying counter-current operation show the trend, that the increase in diafiltration efficiency with increasing diavolumes starts to level off. For an evaluation of the efficiency of a diafiltration system, the applicable protein load per membrane area, e.g. expressed in g/(m² h), is an important aspect in addition to the dilution efficiency. Therefore, we added exemplary numbers of the predicted load for our module as well as for diafiltration experiments reported in the stated literature. Comparing, e.g. the predicted and reported loads at around four diavolumes, it shows that our system could handle about the same protein load per membrane area as the two-stage counter-current SPTFF setup, however at a better dilution

efficiency. The dialysis system achieves even better dilution efficiencies, however, at the expense of protein loads which are around an order of magnitude lower. If dilution efficiencies beyond 99.7% are required, the simulation predicts a relatively sharp decrease of the permitted protein load of our module, dropping below 20 g/(m^2 h) beyond approx. 6.5 diavolumes.

Up to this point all validation experiments and simulation runs shown in Fig.9 have been conducted at a protein concentration of 5 g/L in the feed stream. However, while this concentration range might be encountered in the course of a required diafiltration between e.g. two ion exchange chromatography steps, the normal operation of diafiltration in the course of product formulation encounters protein concentrations in the range of 50 - 100 g/L. Therefore, the question remains if the developed model is able to predict the performance of our SPTFF module also at higher protein concentrations. To answer this question, we performed experiments at 20 g/L and 50 g/L with at a feed flow rate of 0.2 ml/min and unidirectional DF buffer flow at two diavolumes. The developed SPTFF module could handle the increased feed concentrations without problems, achieving diafiltration efficiencies of 78.7% and 79.4%, for 20 g/L and 50 g/L respectively. Without introducing any changes to the developed model, the simulation of these experiments resulted in a predicted diafiltration efficiency of 79.5% in both cases, showing that the model delivers reliable predictions also in the case of higher protein concentrations. The results also show that, at least within the investigated parameter range, the protein concentration in the feed has only a very minor influence onto the achievable diafiltration efficiencies if the feed flux and the number of diavolumes are kept constant. This consistency of the achievable diafiltration efficiency is within our expectation, because the operation of our module is controlled by fixed flow rates of feed, retentate and diafiltration buffer. Increased protein concentrations result in higher transmembrane pressures in the middle part, however, due to the constant flow rates the flow profile and the resulting diafiltration efficiency remain unchanged. Regarding the observed transmembrane pressures, the experiments slightly exceed the simulation results by about 0.3 bar. Nevertheless, even in the case of a feed concentration of 50 g/L, the pressure in the module did not exceed 1 bar throughout the experiment (see Fig S12 in the SI). Therefore, the choice of only two diavolumes has been conservative and it is likely that a higher number diavolumes of approx. three could be applied in case of the selected feed flow rate. In order to reach six or more diavolumes, corresponding to diafiltration efficiencies above 99%, at feed concentrations of 50 g/L, the membrane area of the module would have to be approximately doubled or the feed flow rate would have to been halved.

4 Conclusion and outlook

In this work, a 2D finite element model of our recently developed SPTFF module for continuous diafiltration was developed. The unconventional module contains two membranes allowing a simultaneous withdrawal of permeate and delivery of fresh DF buffer, throughout the whole flow path of the retentate.

The module allows a unidirectional flow of DF buffer through the membrane as well as an operation mode applying an alternating flow direction of DF buffer, switching periodically at certain intervals. Especially, the second operation mode results in a complex hydrodynamic behavior and dynamically changing concentration profiles within the module. The purpose of the model was to predict the diafiltration efficiency in dependence of various operation parameters and to elucidate the dynamic concentration polarization and pressure built-up phenomena. Different from common UF models often applying a resistance-in-series approach, a porous boundary layer above the membrane was introduced, where accumulated macromolecules, such as proteins, result in an increased pressure drop when a convective flow is forced through the boundary layer. A direct correlation between the protein concentration and the resulting pressure drop is achieved by introducing a hypothetical viscosity. The dependence of this hypothetical viscosity on the protein concentration is purely empirical, however, after fitting once to the experimental results, the fixed correlation is able to predict the dynamic pressure within the module at good accuracy for various conditions. Besides the simulated pressures, also the simulated diafiltration efficiencies are in good accordance to the experimental results. The results show that for a fixed number of diavolumes longer intervals between switch the flow direction of the DF buffer correspond to higher diafiltration efficiencies. Therefore, on the one hand frequent switching is detrimental to the performance of module, on the other hand it limits the pressure-built and allows higher flow rates of DF buffer without exceeding the pressure limit of the system. A thorough, computer-based analysis of this antagonistic effects showed that, at least within the investigated parameter range, the first effect prevails and the module achieves its best performance in case of unidirectional DF buffer flow. While from a scientific view it may have been more interesting if an optimum would exist for dynamic alternating conditions, the operation with unidirectional flow strongly simplifies the setup and control of the new SPTFF module, thus increasing its commercial potential. As illustrated in the comparison with other setups for continuous diafiltration, the presented single module approaches the diafiltration efficiency of a counter-current multistage setup applying three conventional SPTFF modules. Although, most experiments and simulations in this work have been conducted for a protein concentration in the feed of 5 g/L, first results at concentrations of 20 and 50 g/L indicate that the developed SPTFF module also can handle higher protein concentrations, as they are encountered e.g. during formulation steps.

Reference

[1]   C. Gavazzi-April, S. Benoit, A. Doyen, M. Britten, Y. Pouliot, Preparation of milk protein concentrates by ultrafiltration and continuous diafiltration : Effect of process design on overall efficiency, J. Dairy Sci. 101 (2018) 9670–9679. https://doi.org/10.3168/jds.2018-14430.

[2]   C. Casey, T. Gallos, Y. Alekseev, E. Ayturk, S. Pearl, Protein concentration with single-pass tangential flow filtration (SPTFF), J. Memb. Sci. 384 (2011) 82–88. https://doi.org/10.1016/j.memsci.2011.09.004.

[3]   E. Iritani, Y. Mukai, E. Hagihara, Measurements and evaluation of concentration distributions in filter cake formed in dead-end ultrafiltration of protein solutions, Chem. Eng. Sci. 57 (2002) 53–62. https://doi.org/10.1016/S0009-2509(01)00362-1.

[4]   S.P. Agashichev, Modelling temperature and concentration polarization phenomena in ultrafiltration of non-newtonian fluids under non-isothermal conditions, Sep. Purif. Technol. 25 (2001) 355–368. https://doi.org/10.1016/S1383-5866(01)00063-6.

[5]   C. Sharma, D. Malhotra, A.S. Rathore, Review of Computational Fluid Dynamics Applications in Biotechnology Processes, (2011). https://doi.org/10.1002/btpr.689.

[6]   R. Wu, K. Su, Z. Wang, T. Hao, S. Liu, A comprehensive investigation of filtration performance in submerged hollow fibre membrane modules with different fibre geometries, Sep. Purif. Technol. 221 (2019) 93–100. https://doi.org/10.1016/j.seppur.2019.03.082.

[7]   A. Reza, C. Moresoli, B. Marcos, Fouling behavior of electroacidified soy protein extracts during cross-flow ultrafiltration using dynamic reversible – irreversible fouling resistances and CFD modeling, J. Memb. Sci. 361 (2010) 191–205. https://doi.org/10.1016/j.memsci.2010.05.057.

[8]   J. Fernández-Sempere, F. Ruiz-Beviá, P. García-Algado, R. Salcedo-Díaz, Visualization and modelling of the polarization layer and a reversible adsorption process in PEG-10000 dead-end ultrafiltration, J. Memb. Sci. 342 (2009) 279–290. https://doi.org/10.1016/j.memsci.2009.06.046.

[9]   T. Chaabane, S. Taha, M. Taleb Ahmed, R. Maachi, G. Dorange, Coupled model of film theory and the Nernst-Planck equation in nanofiltration, Desalination. 206 (2007) 424–432. https://doi.org/10.1016/j.desal.2006.03.577.

[10]   A. Robert van Reis, A.L. Zydney, Membrane Separations in Biotechnology, Curr. Opin. Biotechnol. 12 (2001) 208-211. https://doi.org/10.1016/S0958-1669(00)00201-9.

[11]   E. Iritani, N. Katagiri, Developments of blocking filtration model in membrane filtration, KONA Powder Part. J. 2016 (2016) 179–202. https://doi.org/10.14356/kona.2016024.

[12]   I.M. Griffiths, A. Kumar, P.S. Stewart, A combined network model for membrane fouling, J. Colloid

Interface Sci. 432 (2014) 10–18. https://doi.org/10.1016/j.jcis.2014.06.021.

[13]   A.R. Rajabzadeh, C. Moresoli, B. Marcos, Fouling behavior of electroacidified soy protein extracts during cross-flow ultrafiltration using dynamic reversible-irreversible fouling resistances and CFD modeling, J. Memb. Sci. 361 (2010) 191–205. https://doi.org/10.1016/j.memsci.2010.05.057.

[14]   C. Casey, T. Gallos, Y. Alekseev, E. Ayturk, S. Pearl, Protein concentration with single-pass tangential flow filtration (SPTFF), J. Memb. Sci. 384 (2011) 82–88. https://doi.org/10.1016/j.memsci.2011.09.004.

[15]   J. Dizon-Maspat, J. Bourret, A. D'Agostini, F. Li, Single pass tangential flow filtration to debottleneck downstream processing for therapeutic antibody production, Biotechnol. Bioeng. 109 (2012) 962–970. https://doi.org/10.1002/bit.24377.

[16]   T. Elich, E. Goodrich, H. Lutz, U. Mehta, Investigating the combination of single-pass tangential flow filtration and anion exchange chromatography for intensified mAb polishing, Biotechnol. Prog. 35 (2019). https://doi.org/10.1002/btpr.2862.

[17]   R. Tan, F. Hezel, M. Franzreb, Continuous single pass diafiltration with alternating permeate flow direction for high efficiency buffer exchange, J. Memb. Sci. 619 (2021) 118695. https://doi.org/10.1016/j.memsci.2020.118695.

[18]   M. Haribabu, D.E. Dunstan, G.J.O. Martin, M.R. Davidson, J. Dalton, E. Harvie, Simulating the ultrafiltration of whey proteins isolate using a mixture model, J. Memb. Sci. 613 (2020) 118388. https://doi.org/10.1016/j.memsci.2020.118388.

[19]   R. Ghosh, Study of membrane fouling by BSA using pulsed injection technique, 195 (2002) 115–123. https://doi.org/10.1016/S0376-7388(01)00550-6

[20]   V. Aguirre-Montesdeoca, A.E.M. Janssen, A. Van der Padt, R.M. Boom, Modelling ultrafiltration performance by integrating local (critical) fluxes along the membrane length, J. Memb. Sci. 578 (2019) 111–125. https://doi.org/10.1016/j.memsci.2019.02.040.

[21]   P. Schausberger, N. Norazman, H. Li, V. Chen, A. Friedl, Simulation of protein ultrafiltration using CFD: Comparison of concentration polarisation and fouling effects with filtration and protein adsorption experiments, J. Memb. Sci. 337 (2009) 1–8. https://doi.org/10.1016/j.memsci.2009.03.022.

[22]   B. Marcos, C. Moresoli, J. Skorepova, B. Vaughan, CFD modeling of a transient hollow fiber ultrafiltration system for protein concentration, J. Memb. Sci. 337 (2009) 136–144. https://doi.org/10.1016/j.memsci.2009.03.036.

[23]   M.J. Huter, J. Strube, Model-based design and process optimization of continuous single pass tangential flow filtration focusing on continuous bioprocessing, Processes. (2019). https://doi.org/10.3390/pr7060317.

[24]   M.J. Huter, C. Jensch, J. Strube, Model validation and process design of continuous Single Pass Tangential Flow Filtration focusing on continuous bioprocessing for high protein concentrations, Processes. 7 (2019) 1–18. https://doi.org/10.3390/pr7110781.

[25]   A. Subramani, S. Kim, E.M.V. Hoek, Pressure, flow, and concentration profiles in open and spacer-filled membrane channels, J. Memb. Sci. 277 (2006) 7–17. https://doi.org/10.1016/j.memsci.2005.10.021.

[26]   Z. Wang, K. Su, T. Shu, W. Wang, Numerical simulation of filtration performance in submerged membrane bioreactors: Effect of particle packed structure, Water Sci. Technol. 76 (2017) 2503–2514. https://doi.org/10.2166/wst.2017.426.

[27]   J.P. Quirk, Permeability of porous solids, Trans. Faraday Soc. 57 (1961) 1200-1207. https://doi.org/10.1039/TF9615701200

[28]   S.O. Rastegar, T. Gu, Empirical correlations for axial dispersion coefficient and Peclet number in fixed-bed columns, J. Chromatogr. A. 1490 (2017) 133–137. https://doi.org/10.1016/j.chroma.2017.02.026.

[29]   H. Schmidt-Traub, M. Schulte, A. Seidel-Morgenstern, Preparative Chromatography, second ed., Weinheim, Germany, 2012.

[30]   M.A. Monfared, N. Kasiri, A. Salahi, T. Mohammadi, CFD simulation of baffles arrangement for gelatin-water ultrafiltration in rectangular channel, Desalination. 284 (2012) 288–296. https://doi.org/10.1016/j.desal.2011.09.014.

[31]   C.J. Yehl, M.G. Jabra, A.L. Zydney, Hollow fiber countercurrent dialysis for continuous buffer exchange of high-value biotherapeutics, Biotechnol. Prog. 35 (2019) 1–5. https://doi.org/10.1002/btpr.2763.

[32]   M.G. Jabra, C.J. Yehl, A.L. Zydney, Multistage continuous countercurrent diafiltration for formulation of monoclonal antibodies, Biotechnol. Prog. 35 (2019) 6–11. https://doi.org/10.1002/btpr.2810.

[33]   H. Lutz, Ultrafiltration for Bioprocessing, (2015) 244. https://doi.org/10.1016/B978-1-907568-46-6.00002-1.

[34]   R. Tan, M. Franzreb, Continuous ultrafiltration/diafiltration using a 3D-printed two membrane single pass module, Biotechnol. Bioeng. 117 (2020) 654–661. https://doi.org/10.1002/bit.27233.